Monte Carlo Calculations of Radiative Transfer in the Earth's Atmosphere–Ocean System:

I. Flux in the Atmosphere and Ocean

GILBERT N. PLASS AND GEORGE W. KATTAWAR

Dept. of Physics, Texas A&M University, College Station 77843

ABSTRACT

The upward and downward flux at various levels in the atmosphere and ocean is calculated by a Monte Carlo method which includes all orders of multiple scattering. A realistic model of the atmosphere–ocean system is used. In the atmosphere, both Rayleigh scattering by the molecules and Mie scattering by the aerosols as well as molecular and aerosol absorption are included in the model. Similarly, in the ocean, both Rayleigh scattering by the water molecules and Mie scattering by the hydrosols as well as absorption by the water molecules and hydrosols are considered. Separate single-scattering functions are calculated from the Mie theory for the aerosols and the hydrosols with an appropriate and different size distribution in each case. The scattering angles are determined from the appropriate scattering function including the strong forward-scattering peak when there is aerosol or hydrosol scattering. Both the reflected and refracted rays, as well as the rays that undergo total internal reflection, are followed at the ocean surface, which is assumed smooth. The ocean floor is represented by a Lambert surface. The upward flux as measured either just above the ocean surface or at the top of the atmosphere shows a significant dependence on the turbidity of the ocean water. The upward and downward flux is calculated at various wavelengths from 0.40 to 0.65 μ and for three ocean models: clear, medium turbid, and turbid. The dependence of the flux on the albedo of the ocean floor is presented. The upward as well as the downward flux is larger just below the ocean surface than just above it at those wavelengths with relatively little absorption by water molecules and under those conditions when there is relatively little scattering from the hydrosols. The ratio of the upward to downward flux in the ocean at points away from boundaries is of the order of 0.1 in transparent regions of the spectrum for a clear ocean, but decreases rapidly as either the turbidity or wavelength increases.

1. Introduction

The calculation of the radiation field in the earth's atmosphere–ocean system is a formidable problem. The solar photons undergo scattering and absorption by the atmospheric molecules and aerosols, reflection and refraction at the ocean surface, and further scattering and absorption within the ocean by the water molecules, the hydrosols, and the ocean floor. All parts of this system interact with each other, so that an accurate solution for the radiation field in the ocean cannot be obtained without consideration of the influence of the atmosphere. Similarly, the radiance at the top of the atmosphere, which is now routinely measured from satellites, cannot be calculated with any accuracy for the major fraction of the earth's surface covered by water without consideration of the photon paths within the ocean.

An excellent review of the radiation field in the ocean has been presented by Duntley (1963); a compendium of real data is presented in both tabular and graphic form. Calculations of the radiation field of the atmosphere–ocean system have been made by Waterman and Westell (1956), Ivanoff and Waterman (1958),

Sekera (1961), Neuman and Hollman (1960), and Fraser and Walker (1963), among others. However, it was necessary for all of these authors to make certain simplifying assumptions in their calculations. These include an approximate treatment of multiple scattering, the use of a Rayleigh scattering function for aerosols and hydrosols instead of a more realistic function with strong forward scattering, and the neglect of the influence of the radiation present in one medium upon that in the other. Preisendorfer (1959, 1971) has given a general theory of radiative transfer across a random atmosphere–ocean interface that makes no symplifying assumptions about scattering functions or atmospheric lighting conditions. However, he has not considered the considerable problem of placing these results in a form suitable for numerical computations nor has he obtained any numerical results.

Plass and Kattawar (1969) with the use of Monte Carlo techniques were able to calculate the complete radiation field of the atmosphere–ocean system with a realistic model of each component. In the atmosphere both Rayleigh and aerosol scattering were included in the model, the latter represented by a scattering function with a strong forward peak. Absorption by various

TABLE 1. Cross-section ratios.

Model*	$\lambda(\mu)$	$\dfrac{\sigma_{SR}}{\sigma_{TR}}$	$\dfrac{\sigma_{SM}}{\sigma_{TM}}$	$\dfrac{\sigma_{TR}}{\sigma_T}$
C*	0.40	0.425	0.833	0.537
M	0.40	0.425	0.250	0.0946
T	0.40	0.425	0.152	0.0342
C	0.46	0.588	0.833	0.321
M	0.46	0.588	0.400	0.0637
T	0.46	0.588	0.353	0.0322
C	0.48	0.462	0.833	0.341
M	0.48	0.462	0.435	0.0748
T	0.48	0.462	0.400	0.0397
C	0.50	0.209	0.833	0.496
M	0.50	0.209	0.500	0.150
T	0.50	0.209	0.461	0.0832
C	0.55	0.0735	0.833	0.654
M	0.55	0.0735	0.588	0.286
T	0.55	0.0735	0.562	0.121
C	0.65	0.0110	0.833	0.865
M	0.65	0.0110	0.714	0.622
T	0.65	0.0110	0.346	0.307

* C, clear ocean; M, medium turbid ocean; T, turbid ocean.

atmospheric components including ozone was also taken into account. Both the reflected and refracted rays, as well as the rays that undergo total internal reflection, were followed at the ocean surface. The appropriate absorption and scattering by the water molecules and hydrosols of the ocean were included in the calculation. The scattering function of the hydrosols as calculated by Mie theory from a distribution of sizes agrees well with measurements and has a strong forward maximum. Reflection from the ocean floor was also taken into account where it made an appreciable contribution. The radiation field was obtained by following numerous photons through the atmosphere–ocean system. The Monte Carlo method was used to choose among the many possibilities that may occur at each collision.

These calculations are extended in the present work with a study of the variation of the radiance with wavelength from 0.40 to 0.65 μ and with the cosine of the solar zenith angle μ_0 from 0.15 to 1. Since ocean waters have varying amounts of turbidity, three different models were used at each wavelength to represent a clear, medium turbid, and turbid ocean. The radiance calculated for these wavelengths is given by Kattawar and Plass (1972).

2. Method of calculation

Only a few of the details of the Monte Carlo calculation are given here, since it has already been completely described by Plass and Kattawar (1968, 1969, 1971). The aerosols are represented by spherical particles with a real index of refraction of 1.55 and with radii distributed according to the haze C model proposed by Deirmendjian (1964). In this model the number density is constant when $0.03\,\mu < r < 0.1\,\mu$ and is proportional to r^{-4} for $r \geqslant 0.1\,\mu$, where r is the aerosol radius. The aerosol single-scattering function was calculated from Mie theory by the method discussed by Kattawar

and Plass (1967a, b) and is shown in Fig. 1 of the paper by Plass and Kattawar (1971). The atmosphere was divided into a number of horizontal layers. Rayleigh scattering, aerosol scattering and absorption, and the ozone absorption cross sections were determined for each layer. The aerosol and ozone variations with height were chosen to agree with those of Elterman et al. (1969).

It is more difficult to obtain a satisfactory model for the hydrosols. Our model assumes that the particulate matter can be represented for the purpose of calculation of the scattering function by spheres with $n_1 = 1.15$ and $n_2 = 0.001$, where n_1 and n_2 are the real and imaginary parts, respectively, of the index of refraction with respect to water and with a size distribution which is constant for $r < 1\,\mu$, and proportional to $r^6 \exp(-2r)$ for $r > 1\,\mu$, where r is the radius of the hydrosol. The maximum of this particle size distribution occurs at a particle radius of $3\,\mu$. The single-scattering function was calculated from Mie theory for particles with this size distribution and index of refraction and is shown in Fig. 1 of Plass and Kattawar (1969), where further justification for the use of this single-scattering function is given.

The ocean model is completely specified for the purpose of the Monte Carlo calculation if three cross-section ratios are given at each wavelength. The three required ratios are σ_{SR}/σ_{TR}, σ_{SM}/σ_{TM}, and σ_{TR}/σ_T, where σ_S and σ_T represent scattering and total cross sections, respectively, and R and M represent the Rayleigh and Mie parts of the cross sections. All hydrosol scattering and absorption is included in the Mie part, while all molecular scattering and absorption is included in the Rayleigh part. Values quoted in the literature for these cross sections vary considerably. The values given in Table 1 were finally chosen to be representative of a clear, medium turbid, and turbid ocean at each of the wavelengths considered.

At the atmosphere–ocean interface a random number is used to determine whether a given photon is reflected or transmitted at the surface: the probability for reflection and transmission at a particular angle of incidence is calculated from the Fresnel equations with a refractive index of 1.338. When the photons are incident from below the surface, the calculations take account of total internal reflection for the appropriate angles. The ocean surface was assumed to be smooth in the present calculations.

A brief account of the sequence of events in a typical Monte Carlo calculation is as follows: The position of the first collision of the solar photon is determined. If it is in the atmosphere, random numbers determine from the cross-section ratios for the appropriate atmospheric layer whether it is a Rayleigh (molecular) or Mie (aerosol) collision. The method of statistical weights is used throughout the program (see Plass and Kattawar, 1971) and the absorption is accounted for by simply multiplying the weight by σ_{SR}/σ_{TR} for a

Rayleigh event or by σ_{SM}/σ_{TM} for a Mie event. A photon history is terminated only when the weight falls below some pre-assigned value (taken as 10^{-6} in all calculations reported here). The scattering angle is chosen from the distribution obtained from the single-scattering function for either Rayleigh or aerosol scattering as appropriate. The process is repeated until the photon reaches the atmosphere–ocean surface. From the known probability for reflection at the particular angle of incidence, random numbers are used to decide whether the particular photon is reflected back into the atmosphere or transmitted into the ocean. In either case the appropriate new direction of travel is calculated, taking account of the refraction upon entering the water, if applicable.

When the photon undergoes a collision within the ocean, random numbers determine from the cross-section ratios whether the collision is Rayleigh (molecular) or Mie (hydrosol) and the weight is then modified appropriately to account for absorption. The new scattering angle is determined from the Rayleigh or the hydrosol single-scattering function as appropriate. A typical computer run on the CDC 7600 takes 3 min, during which time 800,000 photon collisions are processed. The results give the upward and downward radiance and flux at 11 different detectors located at various heights in the atmosphere and ocean for six different values for the albedo of the ocean floor.

It should be emphasized that a new scattering angle in three dimensions is calculated from the appropriate scattering functions for each photon collision. In particular, the numerous small-angle scattering events are accurately simulated in the calculation of the photon trajectory. No averaging over angle is done in the calculation of the trajectory. The only averaging in the Monte Carlo method is done at the detectors which record the photons that arrive over various intervals of solid angle.

3. Flux in the atmosphere and ocean

A moderately deep ocean was assumed for these calculations with an optical depth (defined as the product of the number density, total cross section, and vertical distance from ocean surface) $\tau = 10$. The optical depth is always used to specify a point below the ocean surface (taken as $\tau = 0$). It should be noted that an ocean with an optical thickness of $\tau = 10$ has different actual depths for various models at a particular wavelength or for the same model at different wavelengths, since the total cross section depends on the turbidity and wavelength. The calculations were made for six different values of the albedo A of the ocean floor. The upward flux near the ocean floor depends strongly on the value chosen for A. However, the upward flux at other depths and the downward flux are nearly independent of A.

TABLE 2. Flux values.**

Model*	Wave-length (μ)	μ_0	Upward flux at top of atmosphere	Downward flux $A=0$ $\tau=0$	$\tau=10$	Ratio of upward to downward flux at $\tau=3$
C	0.40	1	0.231	0.841	1.70×10^{-3}	8.98×10^{-2}
M	0.40	1	0.205	0.801	2.41×10^{-4}	1.09×10^{-2}
T	0.40	1	0.205	0.797	1.05×10^{-4}	3.14×10^{-3}
C	0.46	1	0.195	0.905	1.19×10^{-2}	1.17×10^{-1}
M	0.46	1	0.157	0.854	1.06×10^{-3}	1.59×10^{-2}
T	0.46	1	0.150	0.853	7.67×10^{-4}	8.26×10^{-3}
C	0.48	1	0.148	0.913	9.00×10^{-3}	9.24×10^{-2}
M	0.48	1	0.130	0.883	1.46×10^{-3}	1.49×10^{-2}
T	0.48	1	0.120	0.880	1.16×10^{-3}	8.93×10^{-3}
C	0.50	1	0.128	0.894	2.11×10^{-3}	4.02×10^{-2}
M	0.50	1	0.119	0.878	1.74×10^{-3}	1.43×10^{-2}
T	0.50	1	0.114	0.877	1.67×10^{-3}	9.55×10^{-3}
C	0.55	1	0.0934	0.881	6.04×10^{-4}	1.45×10^{-2}
M	0.55	1	0.0887	0.884	1.72×10^{-3}	1.17×10^{-2}
T	0.55	1	0.0905	0.880	3.34×10^{-3}	9.98×10^{-3}
C	0.65	1	0.0660	0.909	8.22×10^{-5}	3.25×10^{-3}
M	0.65	1	0.0657	0.912	3.86×10^{-4}	4.42×10^{-3}
T	0.65	1	0.0666	0.907	3.36×10^{-4}	2.85×10^{-3}
C	0.46	0.55	0.302	0.793	6.00×10^{-3}	1.24×10^{-1}
M	0.46	0.55	0.267	0.739	2.97×10^{-4}	1.63×10^{-2}
T	0.46	0.55	0.264	0.737	1.90×10^{-4}	9.22×10^{-3}
C	0.65	0.55	0.137	0.816	2.01×10^{-5}	2.63×10^{-3}
M	0.65	0.55	0.137	0.818	7.11×10^{-5}	4.20×10^{-3}
T	0.65	0.55	0.137	0.818	5.38×10^{-5}	3.25×10^{-3}
C	0.46	0.15	0.561	0.490	3.83×10^{-3}	1.26×10^{-1}
M	0.46	0.15	0.537	0.460	2.22×10^{-4}	1.57×10^{-2}
T	0.46	0.15	0.537	0.456	1.56×10^{-4}	9.82×10^{-3}
C	0.65	0.15	0.372	0.470	8.36×10^{-6}	2.98×10^{-3}
M	0.65	0.15	0.373	0.471	5.17×10^{-5}	4.02×10^{-3}
T	0.65	0.15	0.373	0.470	3.19×10^{-5}	3.59×10^{-3}

* C, clear ocean; M, medium turbid ocean; T, turbid ocean.
** Normalized to unit solar flux perpendicular to incident direction at each wavelength.

Some of the calculated flux values are given in Table 2. The ocean model is listed in the first column, where C is the clear ocean model, M the medium turbid ocean model, and T the turbid ocean model. The wavelength is given in the second column in microns. At each wavelength and for a given model the parameters listed in Table 1 were used for the ocean, while a similar set of parameters was used for the atmosphere that took account of both the wavelength variation of the Rayleigh and aerosol cross sections as well as the variation with height of the aerosol number density. The cosine of the solar zenith angle (μ_0) is listed in column three.

The upward flux at the top of the atmosphere is given in the fourth column of Table 2. This is the flux that would be measured by a satellite over the ocean. This upward flux shows important variations with the turbidity of the ocean water at wavelengths between 0.4 and 0.5 μ. The largest percentage difference occurs near a wavelength of 0.46 μ; the upward flux is 24% greater for the clear ocean model than for the medium turbid model and 30% greater for the clear compared to the turbid model when $\mu_0 = 1$. The percentage differences become smaller as the sun approaches the horizon. It would seem to be possible to obtain important information about the turbidity of ocean water from
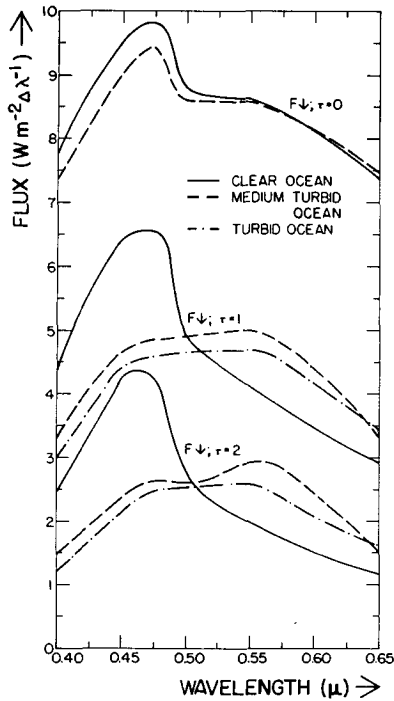
Fig. 1. Downward flux as a function of wavelength for clear, medium turbid, and turbid ocean models. The flux is shown just below the ocean surface ($\tau=0$) and at optical depths of $\tau=1$ and 2. The flux has been multiplied by the solar flux and is given in units of W m^{-2} $\Delta\lambda^{-1}$, where $\Delta\lambda=0.005$ μ.

satellite or airplane flux measurements. In each case the upward flux increases as the solar zenith angle increases; the increased reflectivity of the ocean surface at low solar elevations as well as the increased reflectivity of the aerosol layers cause this flux increase. All of the flux values in Table 2 assume a solar flux of unity independent of wavelength.

The downward flux just beneath the ocean surface ($\tau=0$) is given in the fifth column. At $\lambda=0.46$ μ the downward flux is 6–8% greater for the clear ocean than for the turbid ocean model; the exact value depends on the solar zenith angle. This increase is due to the extra photons in the upward flux for the clear ocean that are totally internally reflected over the appropriate range of angles plus those undergoing reflection at other angles from the underside of the ocean surface; when these upward traveling photons are reflected, they join the downward flux of radiation.

The downward flux just above the ocean floor ($\tau=10$) is given in the sixth column for an albedo $A=0$ of the ocean floor. This is the only column in the table that depends in any appreciable way on the value of A and even this variation is minor as is discussed later. The downward flux decreases as the solar zenith angle increases. At a given wavelength in the transparent region (0.4 $\mu<\lambda<0.5$ μ) the downward flux decreases as the turbidity increases

However the situation is more complicated when

0.5 $\mu<\lambda<0.65$ μ. The downward flux actually increases as the turbidity increases over most of this wavelength range. At first sight this result may seem paradoxical. Two factors combine to cause this variation. First the number of Mie (hydrosol) scattering events increases relative to the Rayleigh (water molecule) events as the turbidity increases; the Mie scattering events send the photons deeper into the ocean than the Rayleigh because of the much greater probability of small-angle scattering around the original direction of the solar beam. Second, there is strong absorption by water at these wavelengths, which is taken into account in the calculation through the Rayleigh absorption cross section. As the turbidity increases, the number of Rayleigh compared to Mie scattering events decreases and the effective absorption decreases at these wavelengths for a given optical thickness. It should be recalled that the actual depth of a $\tau=10$ ocean is less for the turbid than for the clear ocean model.

The ratio of the upward to the downward flux at $\tau=3$ is given in the seventh column of Table 2. This ratio is reasonably constant in the interior of the ocean away from boundaries. The value at $\tau=3$ is typical of this ratio at such interior points. This ratio is of the order of 0.1 in the transparent regions of the spectrum for a clear ocean, but decreases rapidly as the turbidity increases. For $\lambda>0.58$ μ (obtained from interpolation) this ratio first increases and then decreases as the turbidity increases. The combination of varying absorption and forward scattering as discussed in connection with the downward flux causes this variation.
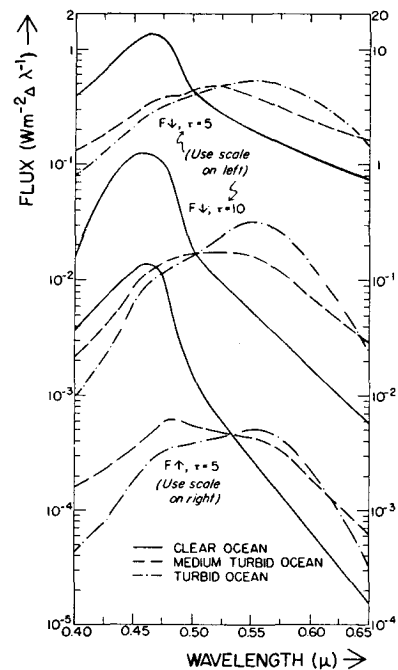

Fig. 2. Downward flux as a function of wavelength at $\tau=5$ and 10 and upward flux at $\tau=5$.

The calculated values listed in Table 2 are for unit solar flux; they were multiplied by an appropriate value for the actual solar flux at the wavelength considered in order to obtain the values shown in our figures. The downward flux (W $m^{-2} \Delta\lambda^{-1}$, where $\Delta\lambda$ =0.005 μ) is shown as a function of wavelength in Fig. 1 for each of the ocean models at $\tau = 0$ (just below the ocean surface), $\tau = 1$ and $\tau = 2$. At $\tau = 0$ the flux is a maximum around $\lambda = 0.47 \mu$. The downward flux is greater for the clear ocean when $\lambda < 0.59 \mu$, but is greater for a turbid ocean when $\lambda > 0.59 \mu$. The flux for the medium turbid and turbid ocean models is the same on the scale of this graph. The downward flux has changed considerably at a depth corresponding to $\tau = 1$. The flux for the clear ocean decreases more rapidly toward longer wavelengths and is less than the flux for the other two models when $\lambda > 0.51 \mu$. The downward flux for the medium turbid and turbid ocean models no longer has a fairly sharp maximum near $\lambda = 0.47\mu$, but instead has a broad flat maximum from $\lambda = 0.45$ to 0.57μ. The curves for $\tau = 2$ show a sharper maximum for the clear ocean model at $\lambda = 0.465 \mu$ and a small maximum for the medium turbid ocean model at $\lambda = 0.56 \mu$.

The downward flux at $\tau = 5$ is plotted in Fig. 2 on a logarithmic scale. The turbid ocean model now shows a maximum at $\lambda = 0.55 \mu$. The downward flux at $\tau = 10$ is plotted for $A = 0$, although the values are very closely the same for other albedos. The flux for the clear ocean model still has a maximum at $\lambda = 0.46 \mu$, while for the turbid ocean model the maximum is at 0.55μ.

The upward flux at the top of the atmosphere is shown in Fig. 3. As already discussed there is an appreciable difference in the values for the clear and turbid ocean models for wavelengths $<0.5 \mu$. The upward flux just above and just below the ocean surface is also given in this figure. The flux just above the
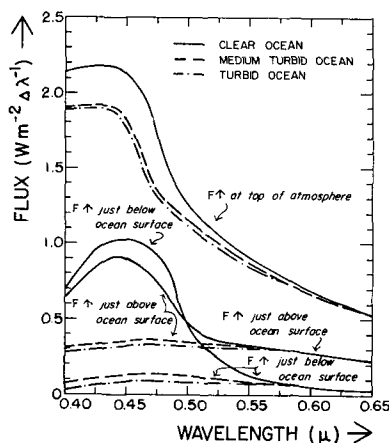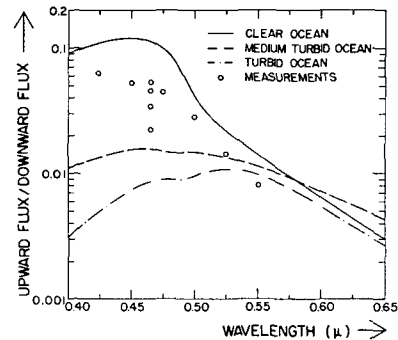

FIG. 4. The ratio of the upward flux to the downward flux at $\tau = 3$ together with experimental measurements of the nadir radiance by Jerlov (1948).

surface is appreciably larger over a clear ocean than over either the medium turbid or turbid ocean at wavelengths $< 0.5 \mu$. Measurements of the upward flux from detectors in aircraft near the ocean surface should show significant differences between waters of varying turbidity.

An interesting feature of Fig. 3 is that the upward flux is greater just below than just above the ocean surface for the clear ocean model when the wavelength is less than 0.5μ. The downward flux, similarly, is greater just below than just above the surface. The difference between the downward and upward flux calculated just above the ocean surface must equal the same quantity calculated just below the surface, as there is no energy loss going through the surface. The downward flux on going through the surface loses photons to the upward flux by reflection from the ocean surface back into the atmosphere. Similarly, the downward flux gains photons just below the surface that are traveling upward and then are reflected from the underside of the ocean surface. The amount lost by the downward flux from reflection back into the atmosphere is always the same for a given solar angle. The amount gained by the downward flux from reflection of the upward flux from the underside of the ocean surface depends on the properties of the ocean. This latter contribution can be greater than the former loss when the water has a low absorption cross section and relatively little hydrosol scattering. These two conditions are satisfied for the clear ocean model when $0.4 \mu < \lambda < 0.5 \mu$. This effect does not occur unless the sun is near the zenith. Our calculations show that both the upward and downward fluxes are smaller below the surface than above when $\mu_0 = 0.55$ and 0.15. When the sun is nearer the horizon, the reflection at the ocean surface increases. The loss from the downward flux from this source can no longer be made up by the gain from reflection of the upward flux within the ocean at the surface.

The upward flux for $\tau = 5$ is shown in Fig. 2. There is a very large variation with wavelength in this flux for the clear ocean model. The upward flux is at least an

FIG. 3. Upward flux as a function of wavelength at the top of of the atmosphere, just above the ocean surface, and just below the ocean surface.
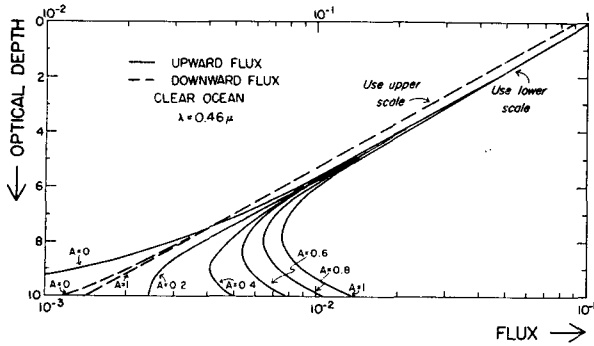
FIG. 5. Upward and downward flux as a function of optical depth for the clear ocean model at $\lambda = 0.46\ \mu$. Curves are given for various values of the albedo A of the ocean floor. Use the upper scale for the downward flux.

FIG. 7. Upward and downward flux as a function of optical depth for the turbid ocean model at $\lambda = 0.46\ \mu$.

order of magnitude larger for the clear than for the medium turbid and turbid ocean models when $\lambda < 0.48\ \mu$. The upward flux becomes smaller as the probability of backscattering decreases (hydrosol scattering increases) and as molecular absorption increases.

The ratio of the upward to the downward flux is given in Fig. 4. This ratio is of the order 0.1 when $\lambda < 0.48\ \mu$ for the clear ocean model, but rapidly decreases at longer wavelengths. The ratio is never larger than 0.016 and 0.011 for the medium turbid and turbid ocean models, respectively. Some experimental measurements of this ratio by Jerlov (1948) are also shown. These measurements are not strictly comparable to the calculations, since the latter are for the flux over the entire hemisphere. The series of points at $\lambda = 0.465\ \mu$ are for waters of varying turbidity. The points seem to agree reasonably well with the theoretical calculations, with only the one at $\lambda = 0.55\ \mu$ lying slightly outside the calculated range.

The upward and downward flux as a function of optical depth is shown in Fig. 5 for the clear ocean model and $\lambda = 0.46\ \mu$. Curves are given for various values for the albedo of the ocean floor. The lower scale should be used for the upward flux and the upper scale for the downward flux. The downward flux shows only a very small dependence on the albedo in the
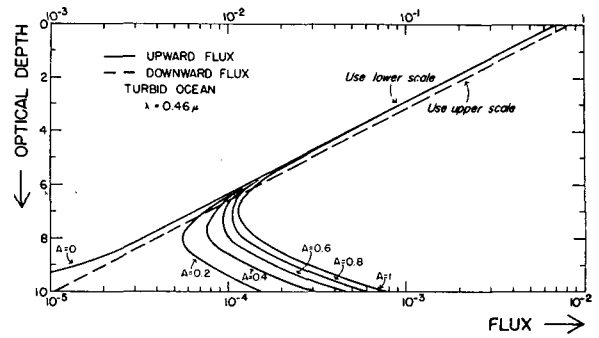
region near the bottom. This is a small effect since the photons reflected from the ocean floor must undergo another scattering event and be scattered in the downward direction before they can contribute to the downward flux. This contribution is a small part of the total downward flux.

On the other hand, the upward flux depends strongly on the albedo in the region near the ocean floor. The upward flux is obviously zero just above the ocean floor when $A = 0$ as no photons are reflected from the floor. The maximum number are reflected when the ocean floor is perfectly reflecting $(A = 1)$. The upward flux when $A = 1$ decreases from the surface down to a minimum value at $\tau = 7.7$ and increases until the ocean floor is reached. The upward flux is nearly independent of A when $\tau < 4$.

The upward and downward flux for the medium turbid and turbid ocean models are given in Figs. 6 and 7, respectively. The dependence of the downward flux on A is very small for these two models and cannot even be shown on the scale of Fig. 7. The upward flux is a much smaller fraction of the downward flux in these two cases than it was for the clear ocean model (note scales at top and bottom of figures). The shape of the curves for the upward flux changes considerably as the turbidity increases. For example, the upward flux for the turbid ocean model when $A = 1$ decreases almost an order of magnitude from the value at the
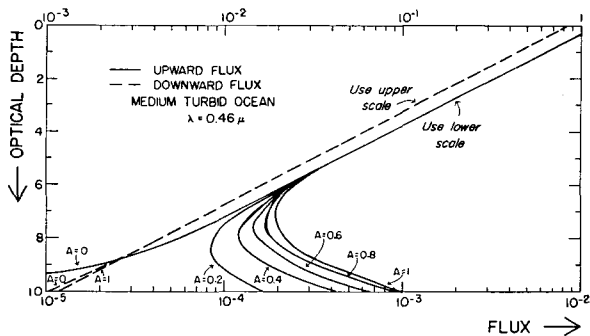

FIG. 6. Upward and downward flux as a function of optical depth for the medium turbid ocean model at $\lambda = 0.46\ \mu$.
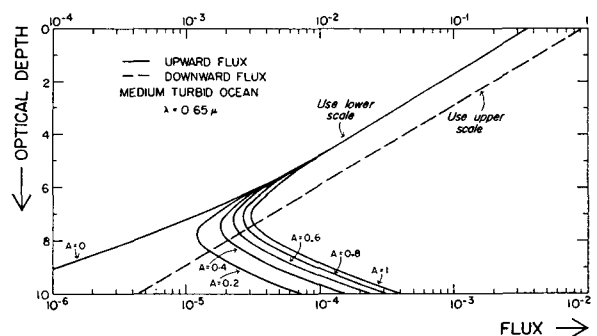

FIG. 8. Upward and downward flux as a function of optical depth for the medium turbid ocean model at $\lambda = 0.65\ \mu$.

ocean floor to the minimum value at $\tau = 7$. Even greater variations occur at wavelengths where water is strongly absorbing, as is shown in Fig. 8 for the medium turbid ocean model with $\lambda = 0.65\ \mu$.

4. Conclusions

The upward and downward flux has been calculated for a realistic model of the atmosphere–ocean system. The results show significant differences in the upward flux depending on the turbidity of the ocean water as measured either just above the ocean surface or even after filtering through the entire atmosphere. The wavelength dependence of both the upward and downward flux at various locations in the atmosphere and ocean is very different for a clear ocean compared to a turbid one. The upward flux (as well as the downward flux) is larger just below the ocean surface than just above it at those wavelengths with relatively little absorption by water molecules $(0.4\ \mu < \lambda < 0.5\ \mu)$ and when there is relatively little scattering from hydrosols (clear ocean model). The dependence of the flux on the albedo of the ocean floor has been calculated. The ratio of the upward to downward flux agrees reasonably well with the reported measurements.

REFERENCES

Deirmendjian, D., 1964: Scattering and polarization properties of water clouds and hazes in the visible infrared. *Appl. Opt.*, **3**, 187–196.

Duntley, S. Q., 1963: Light in the sea. *J. Opt. Soc. Amer.*, **53**, 214–233.

Elterman, L., R. Wexler and D. T. Chang, 1969: Features of tropospheric and stratospheric dust. *Appl. Opt.*, **8**, 893–903.

Fraser, R. S., and W. H. Walker, 1963: Effect of specular reflection at the ground on light scattered from a Rayleigh atmosphere. *J. Opt. Soc. Amer.*, **58**, 636–644.

Ivanoff, A., and T. H. Waterman, 1958: Elliptical polarization of submarine illumination. *J. Marine Res.*, **16**, 283–307.

Jerlov, N. G., 1948: Optical studies of ocean waters. *Rept. Swed. Deep Sea Expedition 1947–1948*, **3**, No. 3.

Kattanar, G. W., and G. V. Plass, 1967a. Electromagnetic scattering from absorbing spheres. *Appl. Opt.*, **6**, 1377–1382.

——, and ——, 1967b. Resonance scattering from absorbing spheres. *Appl. Opt.*, **6**, 1549–1554.

——, and ——, 1972: Radiative transfer in the earth's atmosphere–ocean system: II. Radiance in the atmosphere and ocean. *J. Phys. Oceanog.*, **2**, 146–156.

Neuman, G., and R. Hollman, 1960: On the albedo of the sea surface. *Proc. Symp. Radiant Energy in the Sea*, Intern. Assoc. Phys. Oceanog., 73–83.

Plass, G. N., and G. W. Kattawar, 1968: Monte Carlo calculations of light scattering from clouds. *Appl. Opt.*, **7**, 415–419.

——, and ——, 1969: Radiative transfer in an atmosphere-ocean system. *Appl. Opt.*, **8**, 455–466.

——, and ——, 1971: Radiance and polarization of the earth's atmosphere with haze and clouds. *J. Atmos. Sci.*, **28**, 1187–1198.

Preisendorfer, R. W., 1959: Theoretical proof of the existence of characteristic diffuse light in natural waters. *J. Marine Res.*, **18**, 1–9.

——, 1971: General theory of radiative transfer across the random atmosphere-ocean interface. *J. Quant. Spectry. Radiative Transfer*, **11**, 723–738.

Sekera, Z., 1961: *Union Geodesique et Geophysique Internationale*, Monogr. 10, No. G, Paris, L'Institut Geographique National, 66–72.

Waterman, T. H., and W. E. Estell, 1956: Quantitative effect of the sun's position on submarine light polarization. *J. Marine Res.*, **15**, 149–169.